

# Dark Matter as Perfect Fluid in Low Surface Brightness Galaxies

Xiaobo Gong<sup>1,2,3,4\*</sup>, Zhaoyi Xu<sup>5†</sup>, Meirong Tang<sup>1,2,3,4</sup>

<sup>1</sup>Yunnan Observatories, Chinese Academy of Sciences, 396 Yangfangwang, Guandu District, Kunming, 650216, P.R. China

<sup>2</sup>Key Laboratory for the Structure and Evolution of Celestial Objects, Chinese Academy of Sciences, 396 Yangfangwang, Guandu District, Kunming, 650216, P. R. China

<sup>3</sup>Center for Astronomical Mega-Science, Chinese Academy of Sciences, 20A Datun Road, Chaoyang District, Beijing, 100012, P. R. China

<sup>4</sup>University of Chinese Academy of Sciences, Beijing, 100049, P. R. China

<sup>5</sup>Key Laboratory of Particle Astrophysics, Institute of High Energy Physics, Chinese Academy of Sciences, Beijing 100049, China

## Abstract

When dark matter is a perfect fluid, using the equation of state can get the density profile in the static and spherically symmetric space-time. If the equation of state is independent of the scaling transformation, its lower order approximation can naturally lead to a special case, i.e.  $p = \zeta\rho + 2\epsilon V_{rot}^2\rho$ , where  $p$  and  $\rho$  are the the pressure and density,  $V_{rot}$  is the rotation velocity of galaxy,  $\zeta$  and  $\epsilon$  are positive constants. Then we use this equation of state to derive the mass density profiles of dark matter halos. It can obtain a profile which is similar to the pseudo-isothermal halo model when  $\epsilon$  is around 0.15. It can perfectly fit the observed rotation curves of low surface brightness (LSB) galaxies. When  $\zeta = 0$ , there exists a power law density in the very outer region which surround a black hole, and its power index is  $-\frac{1+4\epsilon}{4\epsilon}$ . The term  $\zeta\rho$  can lead to a constant-density core. If the equation of state include the polytropic model, i.e.  $p = \frac{\zeta}{\rho_0^s}\rho^{1+s} + 2\epsilon V_{rot}^2\rho$ , we can get other kinds of density profiles, such as the profile which is nearly same with the Burkert profile, where  $s$  and  $\rho_0$  are positive constants.

**keywords:** galaxy: dark matter–galaxy: rotation curves

## 1 Introduction

The dark matter are a unsolved puzzle in cosmology and particle physics, and they probably consists of particles that are weakly interacting. Though many astronomical observations, like Cosmic Microwave Background, approximately dark matter makes up 23% of today's Universe. Cosmological models based on cold dark matter in reproducing the large-scale structure of the Universe is quite well and get great success [1]. The most popular candidate for cold dark matter is the weakly interacting massive particles (WIMPs), which are particles with negligible self-interactions, they are stable and collisionless. Their particle masses estimated are in the range  $10 \text{ GeV} \sim 1 \text{ TeV}$ .

However, a plenty of serious challenges to cold dark matter model have emerged on the small scale, such as the scale of individual galaxies and their central core[1]. For example, in the cold dark matter model, halos can be characterized by a power-law mass density distribution with a steep power index at the central core, which is contrary to observation in small scale, such as the observed rotation curves of low surface brightness (LSB) galaxies, which are consist of a very small proportion of ordinary baryonic matter so that their stellar populations make only a relative small contribution to the observed rotation curves, shows that a central constant-density dark matter core exists[2]. Making use of cold dark matter model, numerical N-body simulations can't reproduce a central constant-density dark matter core[3]. This phenomenon is called core-cusp prob-

lem.

There exists many other famous model to explain this core-cusp problem, such as self-interacting dark matter[4] and warm dark matter model[5, 6]. Two of the most canonical candidates for WDM are the sterile neutrino[7] and the gravitino[8]. The dark matter particles are usually classified by their velocity dispersion given in terms of three broad categories: hot (HDM), warm (WDM) and cold (CDM) dark matter. In principle HDM is relativistic at all cosmological relevant scales. When a particle's momentum is equal to or less than its mass (the speed of light are set equal to 1), it become non-relativistic. The warm dark matter have bigger velocity than cold dark matter because of their mass. The typical mass of WDM particle is around 1 KeV. On subgalactic and galactic scales, their non-zero thermal velocities have a strong suppression effect on the steep dark matter power spectrum[6].

In this paper, we want to study the equation of state of dark matter. Because many halo density profiles, like Navarro-Frenk-White (NFW) profile or pseudo-isothermal profile, can be used to fit the density profile of the galaxies from small sizes to large sizes effectively, we can assume that the equation of state is independent of the scaling transformation. Base on the nature of warm dark matter, we think dark matter have a nonzero random motions in the density core. But when dark matter is a perfect fluid, the observations show that the velocity of this random motions is far less than the speed of light. It indicates that dark matter is a dust-like CDM[9, 10]. Taking into account the prop-

\*E-mail: gxbo@ynao.ac.cn

†E-mail: xuzy@ihep.ac.cn

erties of WIMPs, we can assume that random motions of dark matter are positive correlation to the particle rotational motions. In this simple phenomenological model, we can see the dark matter halo profile is in agreement with the observations.

The outline of this paper is as follows. In Section 2 we present two special the equation of state of dark matter and obtain the mass density profiles of dark matter halos. We obtain a approximate analysis to describe the interactive effect between dark matter and black hole in subsection 2.1. In subsection 2.2, we study our above phenomenological model and compare it with the observations. In subsection 2.3, to let the constant random motions vanish at large radius, this term is replaced by the polytropic model. Then we study this new model. In Section 3 we present the conclusions in our work.

## 2 The model

The most general static and spherically symmetric metric takes the following form

$$ds^2 = e^A dt^2 - e^B dr^2 - r^2(d\theta^2 + \sin^2\theta d\phi^2), \quad (1)$$

where  $A$  and  $B$  are function of  $r$ . For conventions, the gravitational constant and the speed of light are set equal to 1. Using the above metric, the Einstein gravitational field equation can be expressed as follows.

$$\begin{aligned} -e^{-B}\left(\frac{1}{r^2} - \frac{B'_r}{r}\right) + \frac{1}{r^2} &= 8\pi T_t^t, \\ -e^{-B}\left(\frac{1}{r^2} + \frac{A'_r}{r}\right) + \frac{1}{r^2} &= 8\pi T_r^r, \\ \frac{-e^{-B}}{2}[A''_{rr} + \frac{(A'_r)^2}{2} + \frac{A'_r - B'_r}{r} - \frac{A'_r B'_r}{2}] &= 8\pi T_\theta^\theta = 8\pi T_\phi^\phi. \end{aligned} \quad (2)$$

Through analyzing the stable circular orbits of a test particle, the rotation velocity  $V_{rot}$  of a test particle can be expressed in the form[11, 9],

$$V_{rot}^2 = \frac{1}{2}rA'_r. \quad (3)$$

If the pure dark matter is an isotropic perfect fluid, its energy momentum tensor takes the form  $T_\nu^\mu = \text{diag}[\rho, -p, -p, -p]$  for the spherically symmetric case. Then we have the following equation

$$N'_x + \left[\frac{F'_x}{2(1+F)} - 2\right]N + \frac{N^2}{2} + \frac{F'_x - 2F}{1+F} = 0. \quad (4)$$

where  $F = e^{-B} - 1$ ,  $N = A'_x$  and  $x = \ln(r)$ . To solve this equation, we need the equation of state(EOS). If pressure  $p$  is only the function of density  $\rho$ , using the following expression

$$\frac{p}{\rho} = -\frac{(1+F)N + F}{F + F'_x}, \quad (5)$$

this lead to  $N$  is a function of  $x, F'_x$  and  $F$ , and mark it as  $N = G(x, F, F'_x)$ . If  $F(r)$  is a solution and  $\lambda$  is a positive constant, then  $F(\lambda r)$  is also its solution. This assumption lead to the equation  $N = G$  doesn't obviously contained  $x$ . It is a autonomous equation. But this also lead to pressure  $p$  is proportional to density  $\rho$ . To take into account more possible EOS, we just assume that  $N$  is a function of  $F'_x$  and  $F$ . The rotation velocity is far less than the speed of light so that  $F$  is very small. When  $F$  and  $F'_x$  are very small, we

can use the Taylor expansion of equation  $G(F, F'_x)$  to stand for it. Because the equation (4) can be solved by iteration,

$$\begin{aligned} N_0 &= -F \\ N_1 &= -F(1 + \frac{3F'_x - 5F - F^2}{4 + 4F - F'_x}) \approx -F(1 + \frac{3}{4}F'_x - \frac{5}{4}F) \\ N_2 &\approx -F(1 - \frac{1}{2}F'_x - \frac{5}{4}F + \frac{3}{8}F''_{xx}) - \frac{3}{8}(F'_x)^2 \\ &\dots \end{aligned} \quad (6)$$

taking into account the above approximate iteration form of variable  $N$ , we consider two case of the Taylor expansion of equation  $N = G(F, F'_x)$  to solve the Equation (4) in the following subsection.

### 2.1 Case I

Using the first iteration formula  $N_1$ , we can assume

$$N = -F + (\gamma F + \epsilon F'_x)F \quad (7)$$

where  $\gamma$  and  $\epsilon$  are constant. This assumption lead to the following equation of state (EOS)

$$p \approx 2\epsilon V_{rot}^2 \rho + \frac{\gamma - \epsilon - 1}{2\pi} \left(\frac{V_{rot}^2}{r}\right)^2 \quad (8)$$

When  $|F| \ll 1$ , and setting  $M = \ln(-F)$ , the Equation (4) can be approximated by

$$2\epsilon U'_x + (4\gamma - 4\epsilon - 3)U + 4\epsilon U^2 + 5 - 4\gamma = 0, \quad (9)$$

where  $U = M'_x$ . This equation is one kind of Riccati Equation. It has two following type of solution. when  $(4\gamma + 4\epsilon - 3)^2 - 32\epsilon > 0$ , one of the solution is

$$F = -\frac{b}{r^{\tilde{\alpha}}} \sqrt{1 + \left(\frac{r}{r_0}\right)^{\tilde{\beta}}}, \quad (\tilde{\beta} > 0) \quad (10)$$

where  $\tilde{\alpha} = \frac{4\gamma - 4\epsilon - 3}{8\epsilon} + \frac{\tilde{\beta}}{4}$ ,  $\tilde{\beta} = \frac{\sqrt{(4\gamma + 4\epsilon - 3)^2 - 32\epsilon}}{2|\epsilon|}$ ,  $b$  and the core radius  $r_0$  are positive constant. Then the density  $\rho$  is

$$\rho = -\frac{F}{8\pi r^2} \left[1 - \tilde{\alpha} + \frac{\tilde{\beta} \left(\frac{r}{r_0}\right)^{\tilde{\beta}}}{2 + 2\left(\frac{r}{r_0}\right)^{\tilde{\beta}}}\right] \quad (11)$$

If density is characterized by a power-law distribution  $\rho \sim r^\alpha$ , i.e.

$$\alpha = \frac{F'_x + F''_{xx}}{F + F'_x} - 2 \quad (12)$$

the absolute value of slope  $\alpha$  should be higher in the outer region. Considering the fact that dark matter density  $\rho$  have lower value and its absolute value of slope  $\alpha$  is higher in the outer region,  $\tilde{\alpha}$  should be equal to 1. This lead to  $\gamma = 1 + \epsilon$ , then it is easy to see that  $p$  is proportional to the term  $V_{rot}^2 \rho$ , i.e.  $p \approx 2\epsilon V_{rot}^2 \rho$ , and the variable  $N$  is given by

$$N = -\frac{F}{1 + F + \epsilon F + \epsilon F'_x}, \quad (13)$$

Thus, Using Equation (2) can leads to the following equation

$$\begin{aligned} 2\epsilon F''_{xx} + F'_x(1 - \epsilon + \frac{\epsilon - 6\epsilon^2 F}{1 + F}) + \frac{\epsilon(F'_x)^2}{F}(1 + \frac{1 + 2\epsilon F'_x}{1 + F}) \\ + (1 - 4\epsilon)F - \frac{4\epsilon^2 F^2}{1 + F} = 0, \end{aligned} \quad (14)$$

and Equation (10) is reduced into the form

$$F = -\frac{b}{r} \sqrt{1 + \left(\frac{r}{r_0}\right)^{\frac{8\epsilon - 1}{2\epsilon}}} \quad (15)$$

When the core radius  $r_0 \rightarrow \infty$ , this solution can become the vacuum Schwarzschild solution and the parameter  $b$  is the Schwarzschild radius in this case. Then the energy density  $\rho$  can be approximated as

$$\rho = \frac{(8\epsilon - 1)b}{32\pi r_0^3} \frac{\left(\frac{r}{r_0}\right)^{\frac{2\epsilon-1}{2\epsilon}}}{\sqrt{1 + \left(\frac{r}{r_0}\right)^{\frac{8\epsilon-1}{2\epsilon}}}} \quad (16)$$

This profile is one of the Zhao halos profile [12], which can acquire both the form of a cusped or a cored profile with three free parameters  $(\bar{\alpha}, \bar{\beta}, \bar{\gamma})$ :

$$\rho = \frac{\rho_0}{\left(\frac{r}{r_0}\right)^{\bar{\gamma}} \left(1 + \left(\frac{r}{r_0}\right)^{\bar{\alpha}}\right)^{\frac{\bar{\beta} + \bar{\gamma}}{\bar{\alpha}}}} \quad (17)$$

When  $r_0$  is very large, there exists a transition zone between density core and outer region when density is characterized by a power-law distribution  $\rho \sim r^\alpha$  for the profile in the Equation (16). The slope is changing from  $\alpha = \frac{2\epsilon-1}{2\epsilon}$  to  $\alpha = -\frac{1+4\epsilon}{4\epsilon}$ . For example, when  $\epsilon = 0.5$ , the density distribution is dominated by a central constant-density core, and is dominated by a outer power-law density distribution  $\rho \sim r^{-1.5}$ . Because in the outer region dark matter have lower density, the interaction force of the dark matter becomes smaller, then variable  $\epsilon$  may be smaller at larger radius, we probably get a more steeper outer power-law density distribution in this more realistic case, like the pseudo-isothermal profile  $\frac{\rho_0}{1 + (r/r_0)^2}$ . Unfortunately, there exists a serious problem. Because  $b$  is the Schwarzschild radius of black hole, so the mass of dark matter within the core radius is only  $\sqrt{2} - 1$  times the black hole mass. The core radius is far less than 1 kilo-parsec (kpc). This is not consistent with the observation.

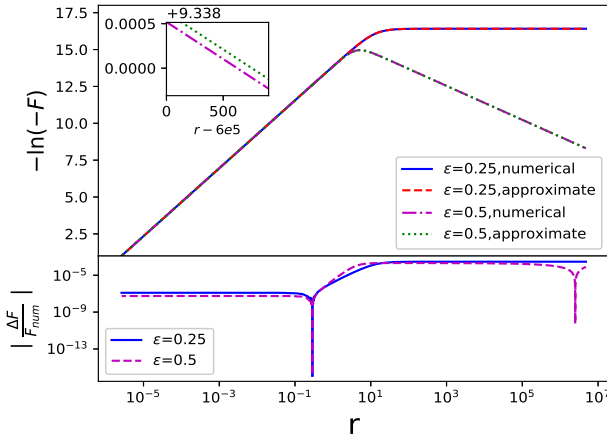


**Figure 1.** Comparison results between the approximate analysis and the numerical solution for  $F$ . **Top:** the result of  $-\ln(-F)$  when  $\epsilon=0.25$  and  $\epsilon=0.5$ . The solid line is for numerical solution when  $\epsilon=0.25$ , The dashed line stands for analysis solution when  $\epsilon=0.25$ . The dash-dotted line is for numerical solution when  $\epsilon=0.5$ . The dotted line is for analysis solution when  $\epsilon=0.5$ . **Bottom:** The relative errors  $(|\frac{\Delta F}{F_{num}}| = |\frac{F_{num} - F_{app}}{F_{num}}|)$  for different  $\epsilon$ .  $F_{num}$  is the numerical solution.  $F_{app}$  is the approximate analysis. The solid line correspond to  $\epsilon=0.25$ , the dashed line is for  $\epsilon=0.5$ .

To test the approximate analysis in the Equation (15), we use the odeint Python routine in the SciPy library to solve the Equation (14). Because the energy density  $\rho$  is not easy to be solved by Equation (2), using Equation (2)

and Equation (14), the energy density  $\rho$  can be rewritten as

$$\begin{aligned} \ln(8\pi r^2 \rho)'_x &= \frac{F''_{xx} + F'_x}{F'_x + F} \\ &= -\frac{1}{2\epsilon} \left[ 1 - 4\epsilon + \frac{\epsilon F'_x}{F} + \frac{\epsilon F'_x}{F(1+F)} - \frac{2\epsilon^2 F'_x}{1+F} + \frac{2\epsilon^2 (F'_x)^2}{F(1+F)} \right. \\ &\quad \left. - \frac{4\epsilon^2 F}{1+F} \right]. \end{aligned} \quad (18)$$

Then using the Equation (18) obtains the density  $\rho$ . The Fig. 1 and Fig. 2 show the comparison results between the approximate analysis and the numerical solution. It is obvious to see that their difference is very small.

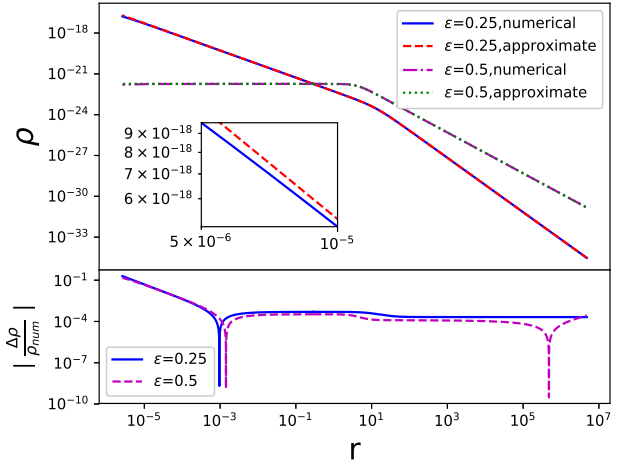


**Figure 2.** Comparison results between the approximate analysis and the numerical solution for  $\rho$ . **Top:** the result of  $\rho$  when  $\epsilon=0.25$  and  $\epsilon=0.5$ . The solid line is for numerical solution when  $\epsilon=0.25$ , The dashed line stands for analysis solution when  $\epsilon=0.25$ . The dash-dotted line is for numerical solution when  $\epsilon=0.5$ . The dotted line is for analysis solution when  $\epsilon=0.5$ . **Bottom:** The relative errors  $(|\frac{\Delta \rho}{\rho_{num}}| = |\frac{\rho_{num} - \rho_{app}}{\rho_{num}}|)$  for different  $\epsilon$ .  $\rho_{num}$  is the numerical solution.  $\rho_{app}$  is the approximate analysis. The solid line correspond to  $\epsilon=0.25$ , the dashed line is for  $\epsilon=0.5$ .

## 2.2 Case II

In the previous case, there don't exist the solution that satisfy the boundary conditions

$$\begin{aligned} F &= 0, \quad \alpha \approx 0 \quad \text{at} \quad r = 0 \\ \alpha &\approx -2 \quad \text{at} \quad r = \infty. \end{aligned} \quad (19)$$

Assume that

$$N = -F - \zeta(F + F'_x) + (1 + \epsilon)F^2 + \epsilon F'_x F \quad (20)$$

where  $\zeta$  is a very small positive constant[9, 10]. This assumption lead to the following equation of state (EOS)

$$p \approx \zeta \rho + 2\epsilon V_{rot}^2 \rho \quad (21)$$

The Equation(20) can lead to the following approximate equation:

$$\begin{aligned} (2\epsilon H - 1)H''_{xx} + (1 + H)H'_x + 2\epsilon(H'_x)^2 \\ + 2H + (1 - 4\epsilon)H^2 = 0. \end{aligned} \quad (22)$$

Where  $H = \frac{F}{2\zeta}$ . When  $|F| \ll \zeta$ , this case lead to the following approximate equation

$$F''_{xx} - F'_x - 2F = 0. \quad (23)$$

Then its solution is

$$F = -\frac{b}{r} - \left(\frac{r}{r_0}\right)^2 \quad (24)$$

where  $b$  and  $r_0$  are constant. This solution can include a black hole and a constant-density core. When  $\zeta \ll |F| \ll 1$ ,  $\epsilon \geq \frac{1}{4}$  and  $F'_x = \chi F$ , this lead to

$$\chi = \frac{4\epsilon - 1}{4\epsilon} \quad \text{or} \quad \alpha = -\frac{4\epsilon + 1}{4\epsilon}. \quad (25)$$

Because it is hard to get the analytical solution of Equation(4) and Equation(20), so the numerical solutions are necessary. The initial condition is  $F = -(\frac{r}{r_0})^2$ . Then the power index  $\alpha$  for the numerical solutions are showed in Fig. 3. The observed data are also showed. The observed LSB sample involves 48 galaxies, which are from de Blok et al. (2001)[2]. These numerical models can perfect response the observed result. The pseudo-isothermal halo model is also showed by the dash-dotted line in Fig. 3. The numerical solution with  $\epsilon = 0.15$  is nearly same with the pseudo-isothermal halo model.

The rotation velocity  $V_{rot}$  is approximately equal to  $\sqrt{-\frac{F}{2}}$  when  $|F| \ll 1$  and  $\zeta \ll 1$ . The numerical solutions with  $\epsilon = 0.5, 0.25, 0.15$  are used in fitting the observed rotation curves.  $r_0$  and  $\zeta$  are adjustable parameters. The observed rotation curves of LSB galaxies are from Kuzio de Naray et al. (2006, 2008, 2010)[13, 14, 15]. The data are fitted by using the least-squares method. The fitting results are showed in Fig. 4. The best fit parameter  $\zeta$  and the reduced chi-square value  $\chi^2_\nu$  are listed in Table 1, and  $\zeta$  is expressed in SI units.

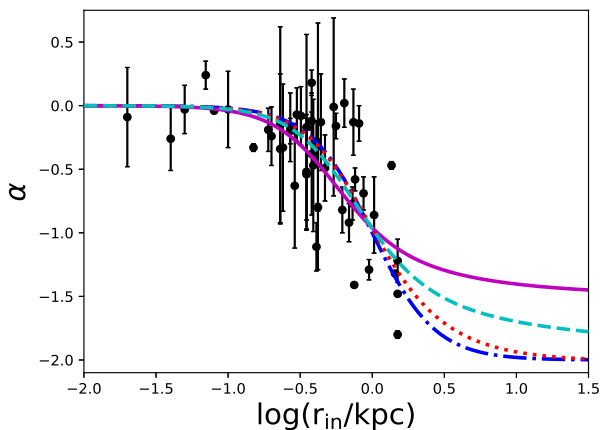


**Figure 3.** Comparison results between the numerical profile in Equation (20) and the pseudo-isothermal profile. The solid line, the dashed line and the dotted line represent the numerical model with  $\zeta = 10^{-6}$  and  $\epsilon = 0.5, 0.25, 0.15$  respectively. The dash-dotted lines is for the pseudo-isothermal model with core radius of 1.0 kpc. Filled circles are the observed data of the slope  $\alpha$ , which are from the de Blok et al. (2001)[2] sample.

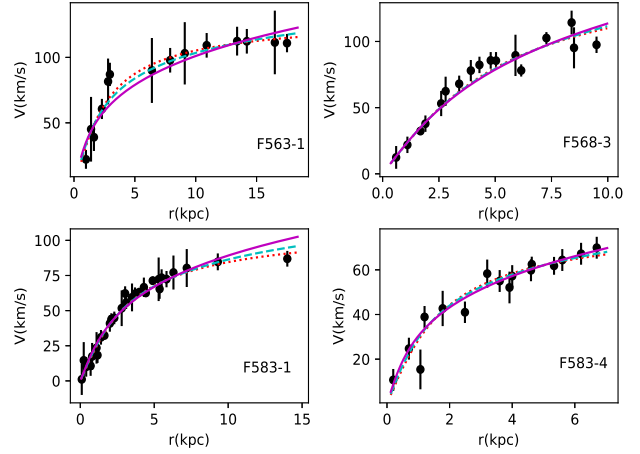


**Figure 4.** Observed LSB galaxy rotation curves with the best-fitting dark matter model. The solid line, the dashed line and the dotted line represent the numerical model with  $\epsilon = 0.5, 0.25, 0.15$  respectively.

If  $\epsilon = 0$ , because  $|F|$  increases with radius as showed in the initial condition, and the term  $F^2$  reduces it, hence  $F'_x = 0$  at  $r = \infty$ [9] (also see Fig. 5). Finally this conditions lead to  $F \approx -4\zeta$  at  $r = \infty$ , i.e. the bigger  $\zeta$  lead to the bigger rotate velocity. If  $\zeta$  is proportional to the square of velocity dispersion at galaxy center, the LSB galaxies with bigger velocity dispersion at galaxy center should have bigger the peak rotation speed ( $V_{max}$ ). This phenomenon has been reported[16]. The velocity dispersion at galaxy center is far less than speed of light in Table 1. It indicates dark matter is cold. The bigger  $\epsilon$  can also lead to bigger  $V_{max}$ . At very outmost region, if  $\rho$  drops rapidly, the term  $\zeta\rho$  may vanish and  $\epsilon$  may become small.

Table 1. The Best-fit parameters.

Galaxy	$\sqrt{\zeta/2}$ (km/s)	$\chi^2_\nu$	$\sqrt{\zeta/2}$ (km/s)	$\chi^2_\nu$	$\sqrt{\zeta/2}$ (km/s)	$\chi^2_\nu$
	$\epsilon = 0.15$		$\epsilon = 0.25$		$\epsilon = 0.5$	
F563-1	41.1 $\pm$ 1.7	0.54	37.5 $\pm$ 2.5	0.72	31.4 $\pm$ 5.4	1.08
F568-3	52.1 $\pm$ 4.4	1.28	54.4 $\pm$ 5.3	1.35	60.5 $\pm$ 7.4	1.47
F583-1	34.7 $\pm$ 1.3	0.48	34.5 $\pm$ 1.6	0.57	34.8 $\pm$ 2.7	0.80
F583-4	26.0 $\pm$ 1.4	0.67	24.5 $\pm$ 1.7	0.59	21.8 $\pm$ 2.6	0.52

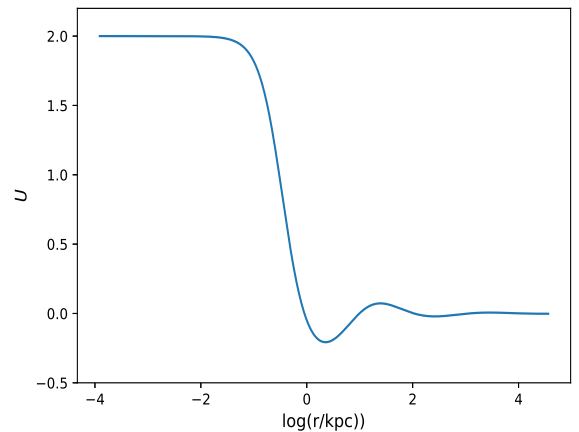


**Figure 5.** The solid line represents  $U$  for the numerical model with  $\zeta = 10^{-6}$  and  $\epsilon = 0$ .

## 2.3 Case III

There exists other density profiles which usually used in LSB galaxies, such as thermal WDM halo density profile[17, 15]

$$\rho = \frac{\rho_0}{[1 + (r/r_0)^2]^\beta}, \quad 1 < \beta \leq \frac{5}{2} \quad (26)$$

and the Burkert profile density profiles[18]

$$\rho = \frac{\rho_0 r_0^3}{(r^2 + r_0^2)(r + r_0)} \quad (27)$$

Their index  $\alpha$  is smaller than -2 in the very outer region. To find similar solution like above profiles, we assume that

$$p = \frac{\zeta}{\rho_0^s} \rho^{1+s} + 2\epsilon V_{rot}^2 \rho, \quad (28)$$

where  $s = \frac{1}{n}$  and  $n$  is the polytropic index. This EOS include the polytropic model. Using the initial condition  $F = -(\frac{r}{r_0})^2$ , we get the numerical solutions of Equation (4) Equation (28). Then the numerical solutions of  $\alpha$  are drawn in Fig. 6. To show clearly, the index  $\alpha$  of Burkert profile minus 0.5 in Fig. 6. When  $n = 5$  and  $\epsilon = 0$ , the polytropic model can get the profile in Equation (26) with  $\beta = 2.5$  in non-relativistic approximation, and it is nearly same with the numerical solution with  $(n, \epsilon) = (1.7, 0.083)$  as showed in Fig. 6. So it exits degeneracy for  $n$  and  $\epsilon$ .

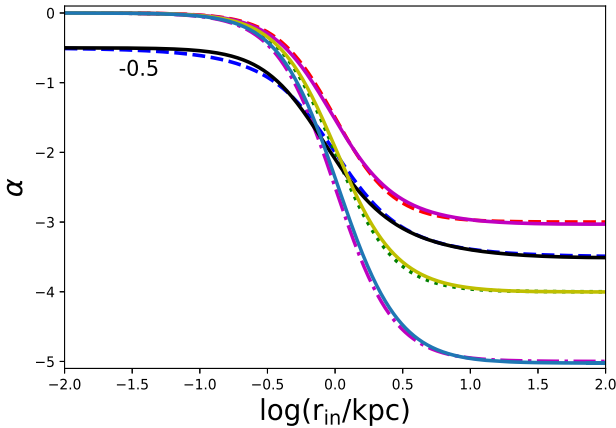


**Figure 6.** The index  $\alpha$  of numerical profile in Equation (28), the profile in Equation (26) and the Burkert profile. The solid lines from upper right to bottom right represent the numerical model with  $\zeta = 10^{-7}$  and  $(n, \epsilon) = (2.3, 0.128), (3.6, 0.109), (1.8, 0.1), (1.7, 0.083)$  respectively. The dashed line at top, the dotted line, the dash-dotted line is for the profile in Equation (26) with core radius of 1.0 kpc and  $\beta = 1.5, 2.0, 2.5$  (from top to bottom). The dashed line at bottom represent the index  $\alpha$  of Burkert profile. To show clearly, the index  $\alpha$  of Burkert profile and the numerical model with  $(n, \epsilon) = (3.6, 0.109)$  minus 0.5.

## 3 Conclusions

In this paper we study EOS of dark matter which treat as a perfect fluid. When EOS is independent of the scaling transformation, it doesn't obviously contained  $x$ . Because the rotation velocity is far less than the speed of light, i.e.  $F$  is very small, we use the Taylor expansion to represent

EOS approximately. Its first order terms can get that the pressure is proportional to density. Its second order terms can naturally yield that random motions of dark matter are correlation to the particle rotational motions. Finally, we get a simplest EOS, i.e.  $p = \zeta\rho + 2\epsilon V_{rot}^2\rho$ .

The term  $\zeta\rho$  can lead to a constant-density core. The constant-density central core can exit in the region with  $|F| \ll \zeta$ . The second order terms in the Taylor expansion can lead to there exists a transition zone between density core and outer region for power index  $\alpha$  when density is characterized by power law relation. So it can obtain a density profile which is similar to the pseudo-isothermal halo model when  $\epsilon$  is around 0.15. By means of the classical least chi square methodology, this profile can perfectly fit the observed rotation curves of LSB galaxies.

When  $\zeta = 0$ , the term  $\epsilon V_{rot}^2\rho$  can get a power law density beyond the region which include a black hole and of which mass is  $\sqrt{2}$  times the black hole mass. The power index  $\alpha$  is  $-\frac{1+4\epsilon}{4\epsilon}$ . When  $\zeta > 0$  and  $\epsilon$  is big, this power law density with  $\alpha = -\frac{4\epsilon+1}{4\epsilon}$  also exit in the very outer region. If  $\zeta$  is proportional to the square of velocity dispersion at galaxy center, then the LSB galaxies with bigger velocity dispersion at galaxy center should have bigger the peak rotation speed.

For the equation of state which include the polytropic model, i.e.  $p = \frac{\zeta}{\rho_0^s} \rho^{1+s} + 2\epsilon V_{rot}^2\rho$ , we can get the density profiles with constant-density core and index  $\alpha$  is less than -2 at very large radius, such as the profile which is nearly same with the Burkert profile.

**Acknowledgements.** This work is supported by the National Natural Science Foundation (NSF) of China (No. 11973081, 11573062, 11403092, 11390374, 11521303), the YIPACAS Foundation (No. 2012048), the Chinese Academy of Sciences (CAS, KJZD-EW-M06-01), the NSF of Yunnan Province (No. 2019FB006) and the Youth Project of Western Light of CAS.

Software: NumPY [19], SciPy [20], Matplotlib [21].

## References

- [1] V. Springel, J. Wang, M. Vogelsberger, A. Ludlow, A. Jenkins, A. Helmi, J. F. Navarro, C. S. Frenk, and S. D. M. White. The Aquarius Project: the subhaloes of galactic haloes. *MNRAS*, 391(4):1685–1711, Dec 2008.
- [2] W. J. G. de Blok, Stacy S. McGaugh, Albert Bosma, and Vera C. Rubin. Mass Density Profiles of Low Surface Brightness Galaxies. *APJ*, 552(1):L23–L26, May 2001.
- [3] Julio F. Navarro, Carlos S. Frenk, and Simon D. M. White. The Structure of Cold Dark Matter Halos. *APJ*, 462:563, May 1996.
- [4] Miguel Rocha, Annika H. G. Peter, James S. Bullock, Manoj Kaplinghat, Shea Garrison-Kimmel, Jose Oñorbe, and Leonidas A. Moustakas. Cosmological simulations with self-interacting dark matter - I. Constant-density cores and substructure. *MNRAS*, 430(1):81–104, Mar 2013.
- [5] Paul Bode, Jeremiah P. Ostriker, and Neil Turok. Halo Formation in Warm Dark Matter Models. *APJ*, 556(1):93–107, July 2001.
- [6] Andrea V. Macciò, Sinziana Paduroiu, Donnino Anderhalden, Aurel Schneider, and Ben Moore. Cores in warm dark matter haloes: a Catch 22 problem. *MNRAS*, 424(2):1105–1112, August 2012.

- [7] A. Boyarsky, M. Drewes, T. Lasserre, S. Mertens, and O. Ruchayskiy. Sterile neutrino dark matter. *Progress in Particle and Nuclear Physics*, 104:1 – 45, 2019.
- [8] Wilfried Buchmüller, Laura Covi, Koichi Hamaguchi, Alejandro Ibarra, and Tsutomu T. Yanagida. Gravitino dark matter in R-parity breaking vacua. *Journal of High Energy Physics*, 2007(3):037, March 2007.
- [9] F. Rahaman, K. K. Nandi, A. Bhadra, M. Kalam, and K. Chakraborty. Perfect fluid dark matter. *Physics Letters B*, 694(1):10–15, October 2010.
- [10] Alexander A. Potapov, Guzel M. Garipova, and Kamal K. Nandi. Revisiting perfect fluid dark matter: Observational constraints from our galaxy. *Physics Letters B*, 753:140–146, February 2016.
- [11] Tonatiuh Matos and Dario Nunez. The general relativistic geometry of the Navarro-Frenk-White model. *arXiv e-prints*, pages astro-ph/0303594, Mar 2003.
- [12] Hongsheng Zhao. Analytical models for galactic nuclei. *MNRAS*, 278(2):488–496, January 1996.
- [13] Rachel Kuzio de Naray, Stacy S. McGaugh, W. J. G. de Blok, and A. Bosma. High-Resolution Optical Velocity Fields of 11 Low Surface Brightness Galaxies. *APJS*, 165(2):461–479, August 2006.
- [14] Rachel Kuzio de Naray, Stacy S. McGaugh, and W. J. G. de Blok. Mass Models for Low Surface Brightness Galaxies with High-Resolution Optical Velocity Fields. *APJ*, 676(2):920–943, April 2008.
- [15] Rachel Kuzio de Naray, Gregory D. Martinez, James S. Bullock, and Manoj Kaplinghat. The Case Against Warm or Self-Interacting Dark Matter as Explanations for Cores in Low Surface Brightness Galaxies. *APJ*, 710(2):L161–L166, February 2010.
- [16] P. Buyle, L. Ferrarese, G. Gentile, H. Dejonghe, M. Baes, and U. Klein. The  $v_c$ - $\sigma_c$  relation in low-mass and low surface brightness galaxies. *MNRAS*, 373(2):700–704, December 2006.
- [17] H. J. de Vega and N. G. Sanchez. The dark matter distribution function and halo thermalization from the Eddington equation in galaxies. *International Journal of Modern Physics A*, 31(13):1650073, May 2016.
- [18] A. Burkert. The Structure of Dark Matter Halos in Dwarf Galaxies. *APJ*, 447:L25–L28, July 1995.
- [19] S. van der Walt, S. C. Colbert, and G. Varoquaux. The numpy array: A structure for efficient numerical computation. *Computing in Science Engineering*, 13(2):22–30, 2011.
- [20] Pauli Virtanen, Ralf Gommers, Travis E. Oliphant, Matt Haberland, Tyler Reddy, David Cournapeau, Evgeni Burovski, Pearu Peterson, Warren Weckesser, Jonathan Bright, and SciPy 1.0 Contributors. SciPy 1.0: Fundamental Algorithms for Scientific Computing in Python. *Nature Methods*, 17:261–272, 2020.
- [21] J. D. Hunter. Matplotlib: A 2d graphics environment. *Computing in Science & Engineering*, 9(3):90–95, 2007.